Journal of Solid State Chemistry 184 (2011) 2553–2558

Contents lists available at ScienceDirect

Journal of Solid State Chemistry

journal homepage: www.elsevier.com/locate/jssc

One-step growth of Si_3N_4 stem–branch featured nanostructures: Morphology control by VS and VLS mode

Qiushi Wang [a], Wei Gao [a], Lianchen Shan [b], Jian Zhang [a], Yunxia Jin [a], Ridong Cong [a], Qiliang Cui [a,*]

[a] State Key Laboratory of Superhard Materials, Jilin University, Changchun 130012, People's Republic of China
[b] Institute of Materials Research (IMO), Hasselt University, Wetenschapspark 1, BE-3590 Diepenbeek, Belgium

ARTICLE INFO

Article history:
Received 14 March 2011
Received in revised form
27 June 2011
Accepted 29 June 2011
Available online 26 July 2011

Keywords:
Silicon nitride
Nanostructure
Arc discharge
Photoluminescence

ABSTRACT

We report here one-step synthesis of Si_3N_4 nanodendrites by selectively applying a vapor–solid (VS) and vapor–liquid–solid (VLS) strategy via direct current arc discharge method. The resultant nanodendrites were characterized by scanning electron microscopy, energy-dispersive X-ray spectroscopy, transmission electron microscopy and X-ray powder diffraction. The spine-shaped nanodendrites were generated by a noncatalytic growth following a VS mode. The uniform secondary nanowire branches were epitaxial grown from two side surfaces of the nanowire stems. The pine-shaped nanodendrites were obtained through a catalytic growth in a VLS process. These branch nanowires were unsystematically grown from the nanocone-like stems. The photoluminescence spectra of the nanodendrites show a strong white light emission around 400–750 nm, suggesting their potential applications in light and electron emission devices.

© 2011 Elsevier Inc. All rights reserved.

1. Introduction

Recently, extensive research efforts have been focused on controlling the morphology, structure, and crystallinity of one dimensional (1D) nanostructures because these parameters have a profound effect on the properties and applications of the materials [1]. Due to their high density interconnects [2], hierarchical 1D nanostructures that possess a distinct stem–branch feature have become research focus recently because of their unique properties and potential applications in gas sensors [3], optics [4,5], energy conversion [6], electronics [7,8], fuel cells [9], solar cells [10] and so on. It is known that the development of hierarchical nanostructures with improved properties depends not only on the alternation of electronic states by creating interfacial regions [11], but also on their morphological arrangement, shape, and crystallographic orientation [12]. Therefore, research toward morphology and structure control of stem–branch featured nanostructures have attracted more and more interest [13].

Si_3N_4 has attracted considerable interest because of its excellent Photoluminescence (PL) and high-temperature mechanical properties [14]. Because of these unique properties and potential applications in nanotechnology, Si_3N_4 nanostructures have been extensively explored through various methods. For example, Si_3N_4 nanobelts were synthesized via a VS thermal reaction between ammonia and SiO [15]. Cao et al. prepared large scaled Si_3N_4 microcoils by CVD method [16]. Si_3N_4 whiskers with novel saw-toothed and riblike structures have been synthesized by a carbothermal reduction and nitridation route [17]. Si_3N_4 nanobelts [18], asymmetric ordered Si_3N_4 nanodendrites [19], Si_3N_4 nanorings [20] and Si_3N_4 nanoplates [21] have been fabricated via catalyst-assisted pyrolysis of polymeric precursors. In this paper, we report the synthesis of Si_3N_4 exhibiting two different hierarchical nanostructures by VS and VLS mode with plasma-assisted direct current (DC) arc discharge method. The spine-shaped nanodendrites were generated by noncatalytic oriented growth following a VS mode, while the pine-shaped nanodendrites were obtained through Fe-catalytic growth in a VLS process. To the best of our knowledge, Si_3N_4 pine-shaped nanodendrites with such morphologies have not been reported. The thin branches, whose diameters were only 20–50 nm, unsystematically grew on the nanocone-like stems and demonstrated complex 3D nanostructures. The characterization of PL revealed that Si_3N_4 nanodendrites owned a broad white light emission band, suggesting their potential applications in light and electron emission devices.

2. Experimental

The spine-shaped nanodendrites were grown in an improved DC arc discharge plasma setup [22]. Differed from a previous system, we designed a graphite sheet as upper substrate located near the anode. A tungsten rod with the purity higher than 99.99%, 8 mm in diameter and 30 cm in length, was used as the cathode. Si (mean size: 200 mesh, purity: 99.95%), SiO_2 (purity: 99.99%) and graphite

* Corresponding author. Fax: +86 431 85168346.
E-mail address: cql@jlu.edu.cn (Q. Cui).

0022-4596/$ - see front matter © 2011 Elsevier Inc. All rights reserved.
doi:10.1016/j.jssc.2011.06.041

powders (purity: 99.99%) were mixed with a molar ratio 1:1:1 in a ball mill and pressed into columns as starting materials. A column, 18 mm in diameter and 4 mm in height, was placed into a water-cooled graphite crucible which acted as the anode. The reaction chamber was first evacuated to less than 1 Pa and then purged with argon several times to remove residual air completely. Then the working gas (N_2, purity: 99.999%) was introduced into the chamber until the inner pressure reached 20 kPa. As the direct current arc discharge was ignited, the discharge voltage was kept in a range of 20–25 V and the discharge current was fixed at 120 A. The discharge process was maintained for 30 min. After passivation in Ar for 6 h, a layer of white-colored flocky product was collected at the graphite sheet.

The growth process of Si_3N_4 pine-shaped nanostructures was also performed as described above. The difference was the usage of Si, SiO_2, graphite and Fe powders (molar ratio: 1:1:1:0.2) as the starting materials. The white powder samples were also collected at the graphite sheet.

The synthesized products were examined initially by using a HITACHI S-4800 scanning electron microscope (SEM) equipped with an energy-dispersive spectrometer (EDS). Further characterization of the nanostructures was carried out using a D8 DISCOVER GADDS powder X-ray diffraction spectrometer (XRD), a JEM-2100F transmission electron microscope (TEM) using an accelerating voltage of 200 kV. The PL spectra were measured with a JY-T800 Raman spectrometer (excited with a He–Cd line at 325 nm). All measurements were performed at room temperature.

3. Results and discussion

The morphology of the obtained deposits was observed using SEM. Fig. 1a is a typical low magnification SEM image of the product. A large amount of spine-shaped nanodendrites were observed. The stems are typically 500–800 nm in diameter and several tens of microns in length. The wire-shaped branches are very uniform in size with diameters of 200–300 nm and distributed at two sides of the stem. Fig. 1b is a high-magnification SEM image of a typical nanodendrite. It can be seen that the branches are nearly perpendicular to the stem. No particles are observed at the tip of stem or the sub-branch, indicating a VS growth mechanism of the nanowires. The EDS analysis (Fig. 2c) reveals that the nanodendrite consists of mainly Si and N. In addition, the nanodendrite also contains a certain amount of O, which is due to surface oxidation. Fig. 1d shows the XRD pattern of the nanodendrite. The diffraction peaks can be well assigned for a hexagonal structure of α-Si_3N_4 with P31c (159) symmetry (based on PDF Card no. 83-0700).

Further detailed morphology and structure are investigated by TEM and selected area electron diffraction (SAED). Fig. 2a is a low magnification TEM image of the nanodendrite. Even after 10 min sonication treatment for the preparation of TEM specimen, the hierarchical structure was not destroyed, indicating that the stem and branches are strongly bonded together. Fig. 2b is the HRTEM image of a representative juncture of the stem and the branches. The parallel lattice fringes can be clearly seen. It can be seen that the branches and stem are virtually one integrated mass. Fig. 2c shows the high-magnification lattice image of the branch. The lattice fringe spacing of 0.67 and 0.56 nm agree well with the (100) and (001) planes of bulk α-Si_3N_4 (PDF Card no. 83-0700). The corresponding SAED patterns (Fig. 2d, e) are identical over the entire stem and branch, indicating that the whole sample is crystalline in nature. The distorted SAED pattern in Fig. 2e is caused by the bending of branch nanowires. The HRTEM and SAED patterns show that, on one hand, the stem grows along $\langle 100 \rangle$ direction, while the branches grow along $\langle 001 \rangle$ direction; on the other hand, the stem and the branch have the same orientation behaviors with their corresponding lattice planes parallel to each other. It is indicated that the branches are epitaxial grown on the stems.

Fig. 3a shows the SEM image of the product synthesized with Si, SiO_2, graphite and Fe powders as precursor. From the typical low magnification SEM images of the sample, it can be seen that

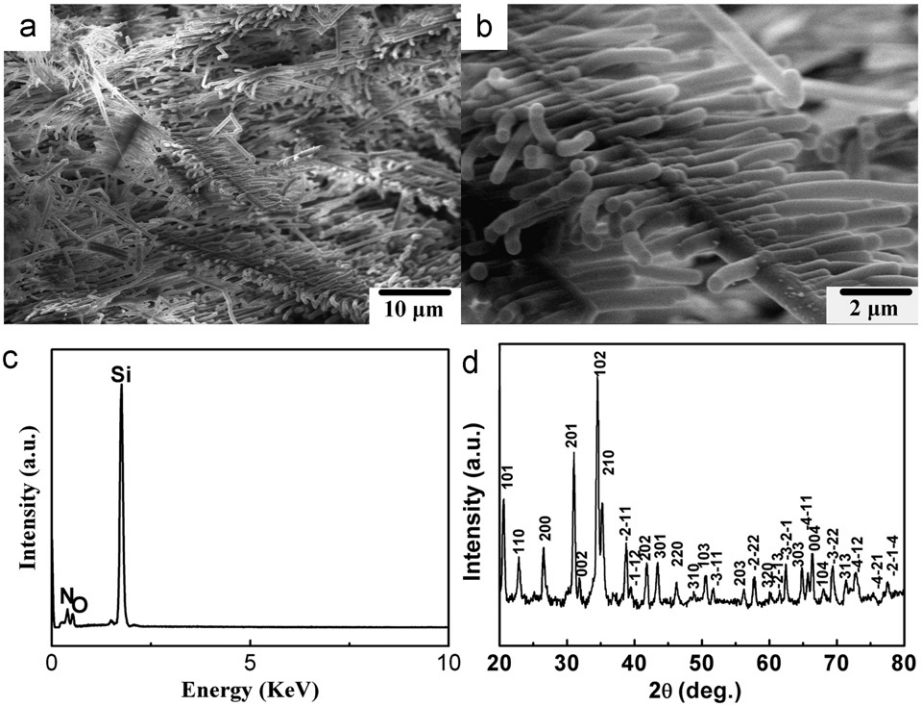

Fig. 1. (a) Low-magnification, (b) high-magnification SEM images, (c) EDS spectrum obtained from the region marked with a rectangle in (b) and (d) XRD pattern of the hierarchical Si_3N_4 nanodendrites.

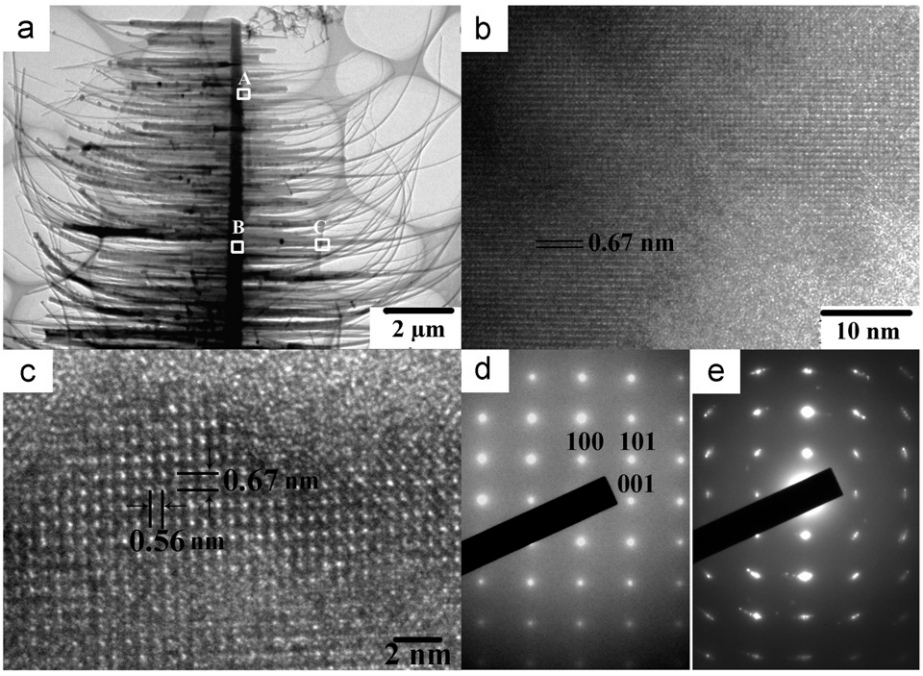

Fig. 2. (a) A TEM image of Si_3N_4 nanodendrites. (b) The HRTEM image of the selected area marked as A in (a). (c) The zoomed-in HRTEM image of a representative juncture of the stem and the branches. (d) The SAED pattern of selected area marked as B. (e) The SAED pattern of selected area marked as C in (a).

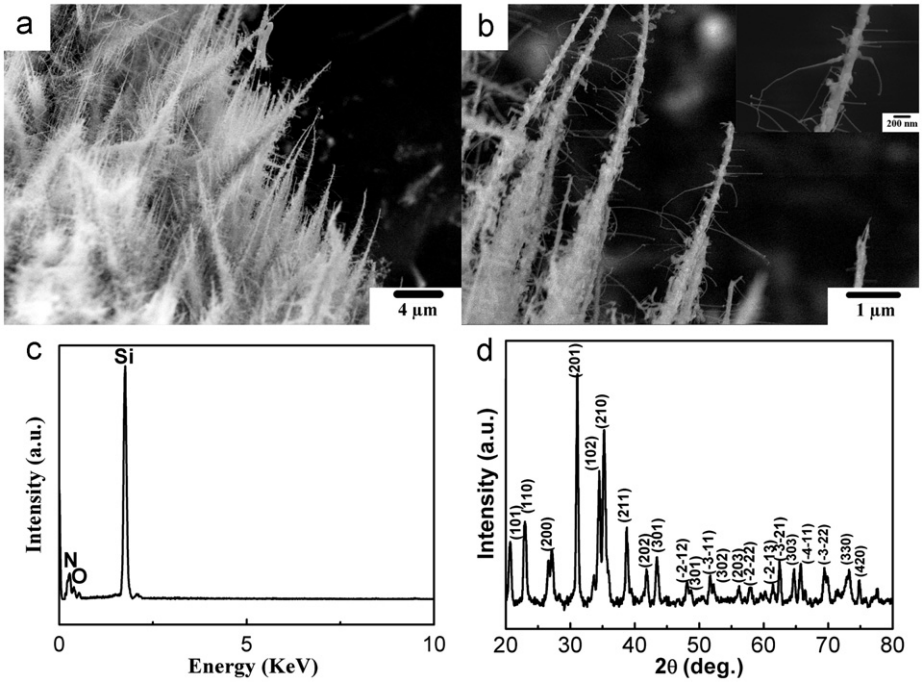

Fig. 3. (a) Low-magnification, (b) high-magnification SEM images, (c) EDS spectrum and (d) XRD pattern of the Si_3N_4 nanodendrites.

the pine-shaped nanodendrites are made up of large quantities of Si_3N_4 nanowires. Fig. 3b is a high-magnification SEM image of a typical stem–branch featured nanostructure. It can be seen that branches are disorderly and unsystematically grown on the surface of the stems. These Si_3N_4 nanocone stems are several micrometers long with the diameters linearly decreasing along the growth direction. The diameter of the branches is, however, only 20–50 nm. In addition, particles can be observed at the tips of each branch nanowires, indicating a VLS growth mechanism of the nanowires. The EDS analysis (Fig. 3c) reveals that the pine-like nanostructure consists of Si, N and a little O. Fig. 3d is a typical XRD pattern of the α-Si_3N_4 products. All peaks can be indexed to the hexagonal α-Si_3N_4 (PDF Card no. 83-0700).

Fig. 4a and b shows TEM image of a typical pine-shaped nanodendrites. The bottom and tip diameters of cone-like stem are about 800 and 100 nm, respectively. The diameters of side branches range from 20 to about 50 nm and the lengths vary from 500 nm to 3 μm. The SAED image indicates that the stem of the nanodendrites is single crystalline, as shown in Fig. 4c. The diffraction pattern can be indexed to α-Si_3N_4. Fig. 4d is the

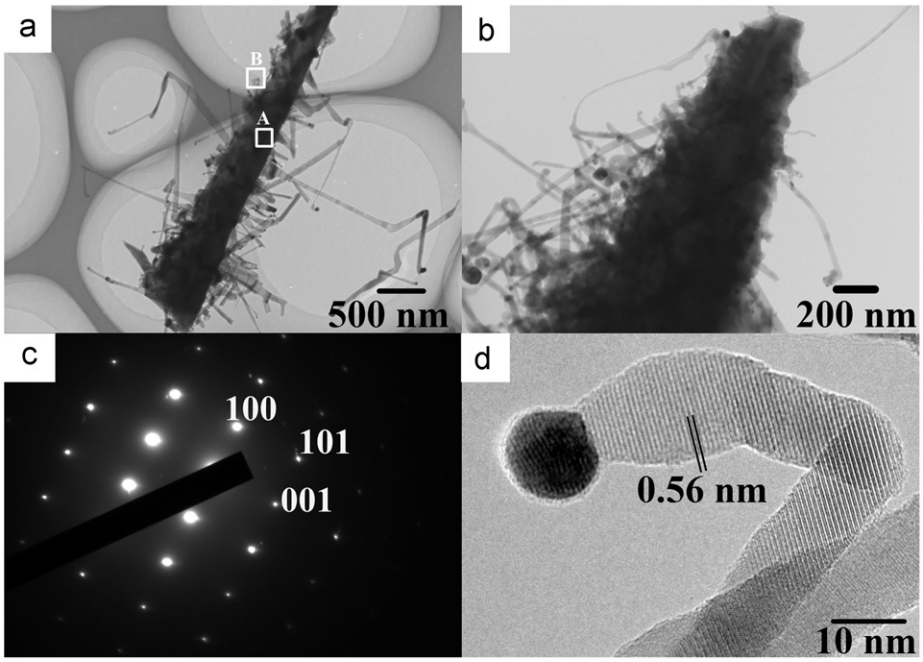

Fig. 4. (a) A TEM image of the bottom of nanodendrites. (b) A TEM image of the top of nanodendrites. (c) The SAED pattern of selected area marked as A in (a). (d) The HRTEM images of selected area marked as B in (a).

HRTEM image of a branch tip. The parallel fringes of the nanowires can be clearly seen, which reveal that the nanobranches are single crystal. In Fig. 4d, the distance between the lattice fringe is measured to be 0.56 nm, which is consistent with the distance of (001) planes of the hexagonal crystal lattice of α-Si_3N_4 with the space group $P31c$ (159) (PDF no. 83-0700). The presence of Fe–Si particles at the tips of branches indicates a Fe-catalytic VLS growth mechanism of the nanowires.

Based on the experimental results, the formation mechanism of Si_3N_4 could be proposed as follows. As soon as the DC arc is ignited, the tungsten rod (cathode) and the source materials (anode) in the graphite crucible are heated to 10^3–10^4 °C. The solid mixture of Si, graphite and SiO_2 is evaporated drastically both thermally by the high temperature and by the bombardment of radicals of the arc zone. The following reactions may proceed among different species simultaneously:

$$SiO_2(s)+Si(s)\rightarrow 2SiO(v)$$

$$SiO_2(s)+C(s)\rightarrow SiO(v)+CO(g)$$

The SiO vapor and CO gases diffuse toward the graphite sheet through an interfacial gas layer. They are adsorbed on the surface of the graphite sheet, where SiO would meet with the reactive radicals generated as a result of the excitation and ionization of flowing N_2. These gaseous species then react with the nitrogenous radicals to form Si_3N_4 and CO_2 via the following reaction [21]:

$$3SiO(v)+3CO(g)+2N_2(g)\rightarrow Si_3N_4(s)+3CO_2(g)$$

To further control the stem–branch featured nanostructures, it is essential to get insight into their growth mechanism. The growth of the spine-shaped nanodendrites is governed by the VS mechanism, while the formation of the pine-shaped nanodendrites follows the VLS mechanism. Based on the above results of observation and analysis, a simple model based on VS epitaxial growth process is proposed for the growth of spine-shaped nanodendrites. The detailed growth procedures of Si_3N_4 spine-shaped nanodendrites are the same as the Si_3N_4 nanocombs which were reported by us before [23]. It has been theoretically established that the possibility of two-dimensional nucleation is related to the surface energy of the crystal, temperature, and vapor supersaturation based on the following equation [24]:

$$P_N = B\exp\left(-\frac{\pi\sigma^2}{K^2T^2\ln\alpha}\right)$$

where P_N is the nucleation possibility, B is a constant, σ is the surface energy, K is the Boltzmann constant, T is the growth temperature, and σ is the vapor supersaturation. The temperature and the vapor supersaturation are two parameters controlled by processing condition. The temperature is invariable, so supersaturation plays an important role for the synthesis of spine-shaped nanodendrites. Firstly, the growth process was mainly a heterogeneous nucleation under low supersaturation condition, which led to preferential growth along the ⟨100⟩ direction with a rapid rate to produce the central axial nanowires. Secondly, with SiO gas accumulated gradually and reaching a steady vapor pressure, the growth process converted from heterogeneous nucleation to homogeneous nucleation. Under this condition, the growth direction of α-Si_3N_4 then switched to ⟨001⟩. The whole growth process of the products can be considered as a combination of the VS mechanism and the secondary epitaxial nucleation mechanism.

Based on the SEM and TEM observations, the pine-shaped nanodendrites morphology is different from the spine-shaped nanodendrites. In the experiments, Fe plays an important role for the synthesis of pine-shaped nanodendrites. It is assumed here that the growth of the stems and branches is dominated by the catalyst-assisted VLS mechanism, although we did not find any particles attached to the tip of stems. Importantly, without the usage of Fe, no hierarchical pine-shaped Si_3N_4 nanodendrites could be obtained. Briefly, at a high reaction temperature in the arc zone, SiO vapors generated by a carbothermal reduction of SiO_2 and graphite powders were transported on the graphite sheet. The SiO vapors reacted with Fe to form Fe–Si–O eutectic liquid droplets on the surface of the graphite sheet, providing energetically favored sites for condensation and absorption of silicon and oxygen species from the vapor phase. The O atoms

which are formed in larger clusters prefer to migrate from the centers to the exterior surfaces, leading to the formation of Fe–Si eutectic liquid cores. At the beginning of the process, the Si and N atoms diffused into the liquid Fe–Si droplets to form the Si_3N_4 stem nanowires, however, the Si and N atoms released on the surface diffuse to the sides of nanowires where they nucleate and form Si_3N_4 crystallites gradually by the "step-flow" mode on the exposed planes of the Si_3N_4 nanowires. And when the temperature is high enough to support vapor-phase epitaxy (VPE) in addition to VLS, this deposition process will occur at the sidewalls of the wires, resulting in the cone shapes. The growth mechanism of Si_3N_4 cone-shaped stem is the same as the growth model in which the VLS growth and VPE growth mechanisms are combined for the formation of the III-V nanocone [25,26]. This model is helpful to understand the unique phenomena in our experiments. Later, the Fe–Si catalyst is no longer visible due to the coverage with Si_3N_4 layers. When the nanocones grow out from the Fe–Si droplets, due to the high surface reactivity and absorptivity, the Fe atoms in the vicinity around the nanocones are transferred to their amorphous SiO_x layer surfaces, playing the role of new nucleation centers for the growth of branches via the mechanism of VLS. Therefore, we propose that the growth of the pine-shaped nanodendrites can be separated into two stages. The first stage was a fast growth of the cone-like stem with the eutectic alloy liquid as the catalyst; the second stage was the branches nucleate and grow on the cone-like stem via VLS mode.

Fig. 5 shows the comparison PL spectra of the Si_3N_4 spine-shaped and pine-shaped nanodendrites, which is excited by 325 nm UV light from He–Cd laser at room temperature. Intensive light emission of the Si_3N_4 nanodendrites was observed even with naked eyes. Both samples show broad emissions ranging from around 450 to 700 nm with maximum peaks centered at 522 nm. Previously, Robertson's [27] studies on Si_3N_4 show that there are four types of defects: Si–Si and N–N bonds, and Si and N dangling bonds. The Si–Si bond forms a bonding σ orbital and antibonding σ^* orbital that are separated by 4.6 eV in stoichiometric Si_3N_4. The silicon dangling bond forms a gap state about midgap, and the two nitrogen defect states that give rise to levels within the gap, namely, N_4^+ and N_2^0, are near the conduction and valence bands, respectively. In this model, the PL peak at 522 nm is related to the inherent imperfect Si and N dangling bonds in the α-Si_3N_4. This peak is the same as in previous work on α-Si_3N_4 nanowires formed by the reaction of Mg_3N_2 and $SiCl_4$ at 600 °C [28] (only one peak centered at 525 nm was observed). This result is a little different from previous work on wide α-Si_3N_4 nanobelts formed by VS thermal reaction between SiO and NH_3 [15] (only one peak centered at 575 nm was observed), and from α-Si_3N_4 nanobelts formed by catalytic-assisted pyrolysis of a polymeric precursor [29] (three broad peaks centered at 1.8, 2.3, and 3.0 eV were observed). It is well known that the morphology and size of materials have important effects on material physical properties, so we believe that the blueshift can be attributed to the small thickness of the Si_3N_4 nanodendrites. Of course, the detailed mechanism of PL needs further study. The PL emission indicates that the stem–branch featured nanostructure of Si_3N_4 may have potential applications in light and electron emission devices.

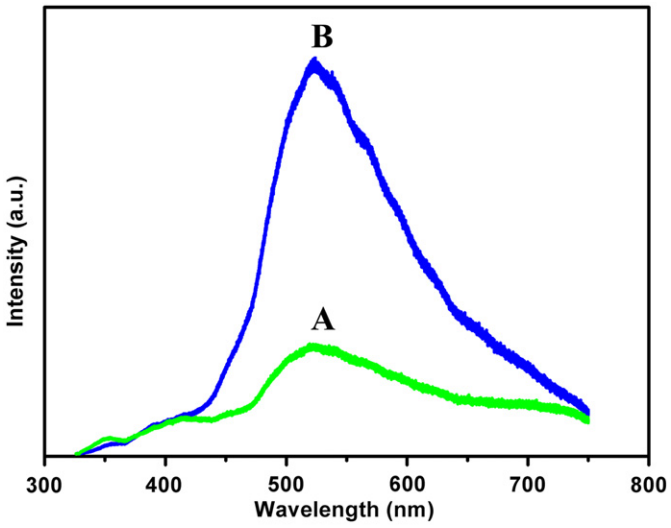

Fig. 5. PL spectrum of the as-synthesized Si_3N_4 nanodendrites: (A) spine-shaped nanodendrites and (B) pine-shaped nanodendrites.

4. Conclusions

In conclusion, we have successfully synthesized two types of nanodendrites by VS and VLS modes. Spine-like nanodendrites were generated by a noncatalytic growth following a VS mode. The growth mechanism is supposed to be dominated by a combination of VS mechanism and the secondary epitaxial nucleation process. The pine-shaped nanodendrites were obtained through a catalytic growth in a VLS process. The growth mechanism is supposed to be dominated by a combination of VLS and VPE mechanism for the stem, and followed by VLS for the branches. This well-controlled synthesis strategy is expected to be applicable to fabrication of other stem–branch featured nanostructures. Room-temperature PL spectra of these nanostructures show broad visible emission around 400–750 nm, which can be attributed to defects in the Si_3N_4 structure.

Acknowledgments

This work is supported by the Research Startup Fund of Jilin University (no. 419080103460), the Natural Science Foundation of China (nos. 50772043 and 11074089) and the National Basic Research Program of China (no. 2011CB808200).

References

[1] J.P. Hill, W.S. Jin, A. Kosaka, T. Fukushima, H. Ichihara, T. Shimomura, K. Ito, T. Hashizume, N. Ishii, T. Aida, Science 304 (2004) 1481–1483.
[2] D. Wang, F. Qian, C. Yang, Z.H. Zhong, C.M. Lieber, Nano Lett. 4 (2004) 871–874.
[3] D.F. Zhang, L.D. Sun, C.J. Jia, Z.G. Yan, L.P. You, C.H. Yan, J. Am. Chem. Soc. 127 (2005) 13492–13493.
[4] W.W. Lei, D. Liu, P.W. Zhu, Q.S. Wang, G. Liang, J. Hao, X.H. Chen, Q.L. Cui, G.T. Zou, J. Phys. Chem. C 112 (2008) 13353–13358.
[5] H.Q. Yan, R.R. He, J. Johnson, M. Law, R.J. Saykally, P.D. Yang, J. Am. Chem. Soc. 125 (2003) 4728–4729.
[6] Y. Qin, X.D. Wang, Z.L. Wang, Nature 451 (2008) 809–814.
[7] Y. Cui, C.M. Lieber, Science 291 (2001) 851–853.
[8] C.Y. Kuan, M.H. Hon, J.M. Chou, I.C. Leu, Cryst. Growth Des. 9 (2009) 813–819.
[9] X. Sun, R. Li, B. Stansfield, J.P. Dodelet, S. Desilets, Chem. Phys. Lett. 394 (2004) 266–270.
[10] L.F. Xu, Q.W. Chen, D.S. Xu, J. Phys. Chem. C 111 (2007) 11560–11565.
[11] M.S. Gudiksen, L.J. Lauhon, J. Wang, D.C. Smith, C.M. Lieber, Nature 415 (2002) 617–620.
[12] A.T. Bell, Science 299 (2003) 1688–1691.
[13] Y. Zhang, R.Y. Li, X.R. Zhou, M. Cai, X.L. Sun, Cryst. Growth Des. 9 (2009) 4230–4234.
[14] W.Y. Yang, H.T. Wang, S.Z. Liu, Z.P. Xie, L.N. An, J. Phys. Chem. B 111 (2007) 4156–4160.
[15] L.W. Yin, Y. Bando, Y.C. Zhu, Y.B. Li, Appl. Phys. Lett. 83 (2003) 3584–3586.
[16] C.B. Cao, H.L. Du, Y.J. Xu, H.S. Zhu, T.H. Zhang, R. Yang, Adv. Mater. 20 (2008) 1738–1743.
[17] Y.J. Xu, C.B. Cao, Z. Chen, J. Li, F.C. Wang, H.N. Cai, J. Phys. Chem. B 110 (2006) 3088–3092.
[18] W.Y. Yang, Z.P. Xie, H.Z. Miao, L.G. Zhang, L.N. An, J. Phys. Chem. B 110 (2006) 3969–3972.

[19] W.Y. Yang, F.M. Gao, H.T. Wang, Z.P. Xie, L.N. An, Cryst. Growth Des. 8 (2008) 2606–2608.
[20] W.Y. Yang, X.M. Cheng, H.T. Wang, Z.P. Xie, F. Xing, L.N. An, Cryst. Growth Des. 8 (2008) 3921–3923.
[21] W.Y. Yang, F.M. Gao, G.D. Wei, L.N. An, Cryst. Growth Des. 10 (2010) 29–31.
[22] J. Zhang, Q.S. Wang, F. Wang, X.H. Chen, W.W. Lei, Q.L. Cui, G.T. Zou, J. Phys. D—Appl. Phys. 42 (2009) 035108.
[23] Q.S. Wang, Q.L. Cui, P.W. Zhu, Y.X. Jin, J.A. Hao, J.A. Zhang, Mater. Res. Bull. 45 (2010) 888–891.
[24] Z.R. Dai, Z.W. Pan, Z.L. Wang, Adv. Funct. Mater. 13 (2003) 9–24.
[25] R.L. Woo, L. Gao, N. Goel, M.K. Hudait, K.L. Wang, S. Kodambaka, R.F. Hicks, Nano Lett. 9 (2009) 2207–2211.
[26] Q.T. Zhou, Y.Q. Chen, Y. Su, C. Jia, B. Peng, S. Yin, S. Li, W.H. Kong, Mater. Res. Bull. 43 (2008) 2207–2212.
[27] J. Robertson, Philos. Mag. B—Phys. Condens. Matter Stat. Mech. Electron. Opt. Magn. Prop. 63 (1991) 47–77.
[28] G.F. Zou, B. Hu, K. Xiong, H. Li, C. Dong, J.B. Liang, Y.T. Qian, Appl. Phys. Lett. 86 (2005) 181901.
[29] L.G. Zhang, H. Jin, W.Y. Yang, Z.P. Xie, H.H. Miao, L.N. An, Appl. Phys. Lett. 86 (2005) 061908.